IEEE MLSP 2025

UNIVERSITY OF ILLINOIS URBANA-CHAMPAIGN

RSR-NF: Neural Field Regularization by Static Restoration Priors for Dynamic Imaging

Berk Iskender[1,3,*], Sushan Nakarni[4], Nitin Daphalapurkar[4], Marc L. Klasky[4], Yoram Bresler[1,2,3]

Depts. of [1]ECE, [2]BioE, and [3]Coordinated Science Lab
University of Illinois, Urbana-Champaign, IL, US

[4]Los Alamos National Laboratory, NM, US

Email: berki2@illinois.edu

*Currently at Analog Garage, Analog Devices, Inc., Boston, MA, US

This research was supported in part by Los Alamos National Labs under Subcontract No. 599416/CW13995

Introduction: Dynamic Tomography

ILLINOIS ECE

Problem: Dynamic object recovery from projections acquired sequentially in time

- **Applications:** medical imaging [1], imaging of fluid flow processes [2,3], micro-CT [4], materials science experiments [5]…

Challenge:

- $\sim N$ projections are required to reconstruct an $N \times N$ static object
- Dynamic object → only $n \ll N$ projections ($n = 1$ in the extreme case) are acquired at any time instant

➡ Highly ill-posed: too few projections to reconstruct the object at any time

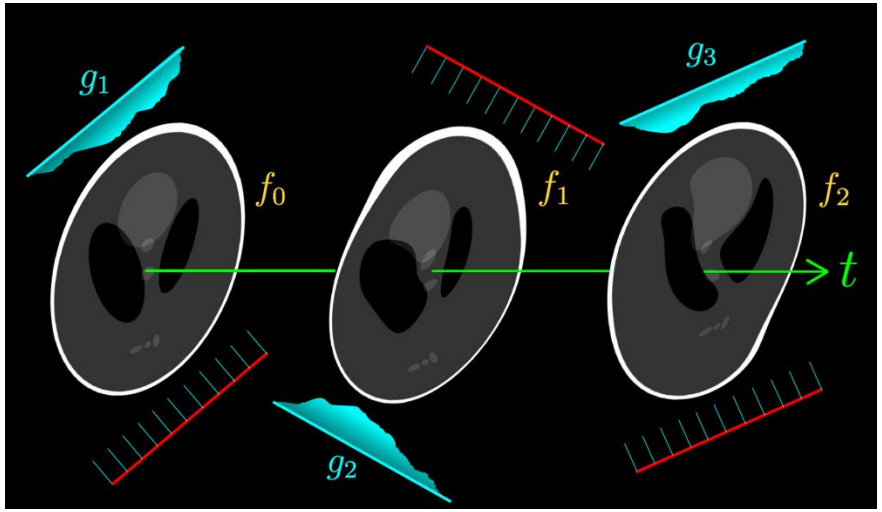

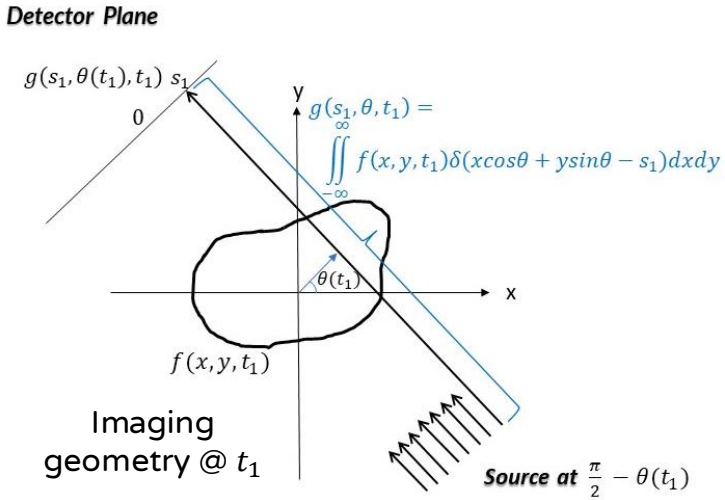

Commercial CT scanner

Compressed Polymer

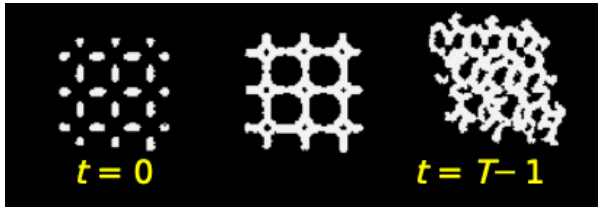

Synthetic piecewise warp of a walnut

Beating heart

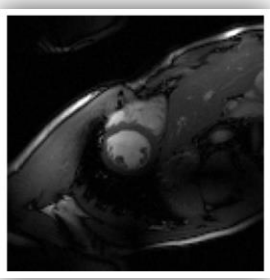

Problem Statement

ILLINOIS ECE

- **Goal:** To reconstruct a time-varying object $f(\mathbf{x}, t),\ \mathbf{x} \in \mathbb{R}^2$, from its projections

$$g(\cdot, \theta, t) = \mathcal{R}_\theta\{f(\mathbf{x}, t)\}$$

Problem Statement

ILLINOIS ECE

- **Goal:** To reconstruct a time-varying object $f(\mathbf{x}, t),\ \mathbf{x} \in \mathbb{R}^2$, from its projections

$$g(\cdot, \theta, t) = \mathcal{R}_\theta\{f(\mathbf{x}, t)\}$$

- **Assumption:** Uniform time-sequential sampling of a **single** angle θ_p at each t_p with sampling scheme $\{\theta_p\}_{p=0}^{P-1}$.

$$\{g(s, \theta_p, t_p)\}_{p=0}^{P-1},\ \forall s, t_p = p\Delta_t$$

$\mathcal{R}_\theta$: The Radon transform operator at angle θ

s: Offset of the line of integration from the origin

P: Total number of projections (and temporal samples)

Δ_t: Time-difference between consecutive projections

Problem Statement

- **Goal:** To reconstruct a time-varying object $f(\mathbf{x}, t),\ \mathbf{x} \in \mathbb{R}^2$, from its projections

$$g(\cdot, \theta, t) = \mathcal{R}_\theta\{f(\mathbf{x}, t)\}$$

- **Assumption:** Uniform time-sequential sampling of a **single** angle θ_p at each t_p with sampling scheme $\{\theta_p\}_{p=0}^{P-1}$

$$\{g(s, \theta_p, t_p)\}_{p=0}^{P-1},\ \forall s, t_p = p\Delta_t$$

- Filtered backprojection (FBP) for reconstruction leads to severe artifacts

$\mathcal{R}_\theta$: The Radon transform operator at angle θ

s: Offset of the line of integration from the origin

P: Total number of projections (and temporal samples)

Δ_t: Time-difference between consecutive projections

Brain CT

Severe motion artifact*

Static

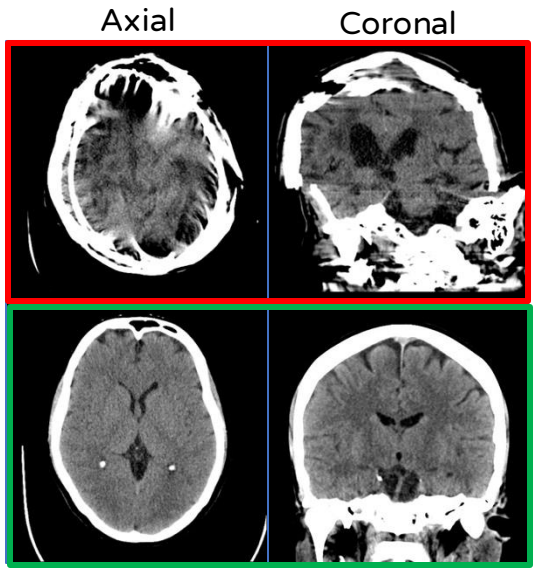

Synthetically warped walnut reconstructed using a single projection at a time

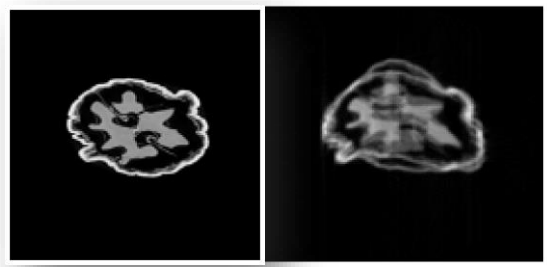

f FBP Recon

*Case courtesy of Dr David Cuete, Radiopaedia.org, rID: 25637

Prior Works

Prior Works

- Joint estimation of the motion field & object[1]
- PDE-based motion field estimation[2]

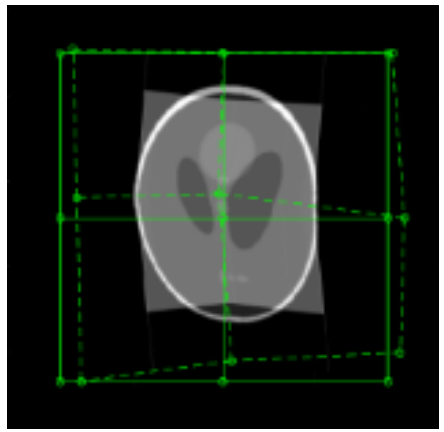

➢ Assume fixed total density at different times

➢ Unable to represent topological changes

[1] [Jailin and Roux, 2018, Jailin et al., 2021, Zang et al., 2018, Capostagno et al., 2021], [2] [Burger et al., 2017, Hahn et al., 2022], [3] [Liang, 2007, Haldar and Liang, 2010, Zhao et al., 2012, Lingala and Jacob, 2013], [4] [Gao et al., 2011, Lingala et al., 2011, Otazo et al., 2015, Ravishankar et al., 2017, Babu et al., 2023]

Prior Works

- Joint estimation of the motion field & object[1]
- PDE-based motion field estimation[2]

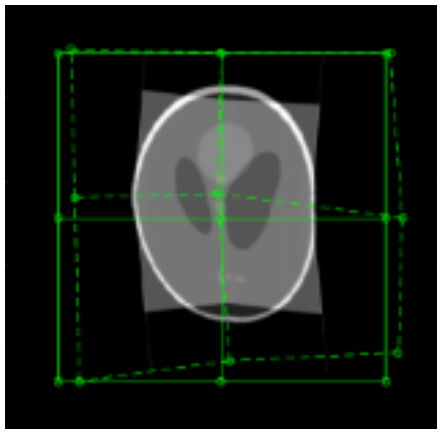

➢ Assume fixed total density at different times

➢ Unable to represent topological changes

- Low-rank, partially separable models (PSM)[3]

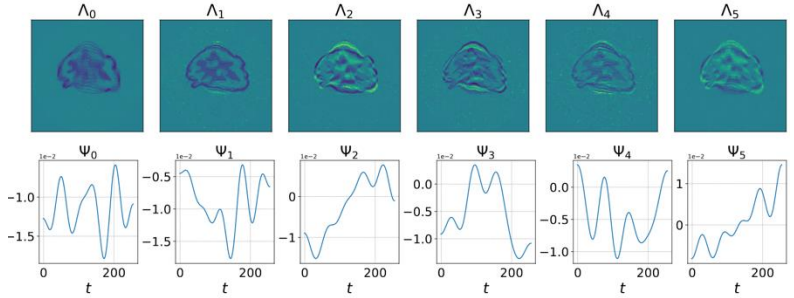

➢ Simple spatio-temporal priors

➢ Memory requirement & number of free parameters scale with the object resolution

➢ Hard-constraint low-rank prior not sufficiently expressive for highly dynamic objects

[1] *[Jailin and Roux, 2018, Jailin et al., 2021, Zang et al., 2018, Capostagno et al., 2021]*, [2] *[Burger et al., 2017, Hahn et al., 2022]*, [3] *[Liang, 2007, Haldar and Liang, 2010, Zhao et al., 2012, Lingala and Jacob, 2013]*, [4] *[Gao et al., 2011, Lingala et al., 2011, Otazo et al., 2015, Ravishankar et al., 2017, Babu et al., 2023]*

Prior Works

- Joint estimation of the motion field & object[1]
- PDE-based motion field estimation[2]

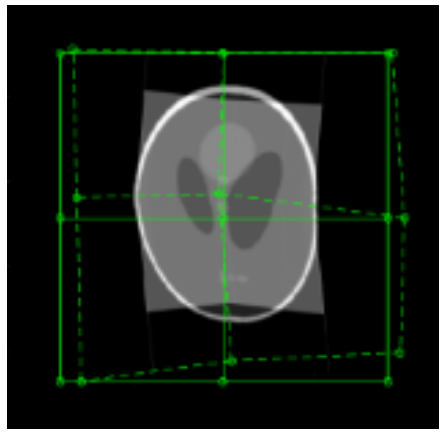

➢ Assume fixed total density at different times

➢ Unable to represent topological changes

- Low-rank, partially separable models (PSM)[3]

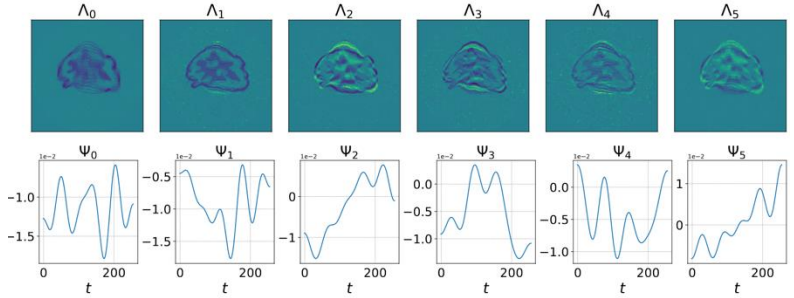

➢ Simple spatio-temporal priors

➢ Memory requirement & number of free parameters scale with the object resolution

➢ Hard-constraint low-rank prior not sufficiently expressive for highly dynamic objects

- Implicit LR promoting methods[4]

➢ Require full-rank representation

➢ Memory requirement & number of free parameters scale with the object resolution

[1] *[Jailin and Roux, 2018, Jailin et al., 2021, Zang et al., 2018, Capostagno et al., 2021]*, [2] *[Burger et al., 2017, Hahn et al., 2022]*, [3] *[Liang, 2007, Haldar and Liang, 2010, Zhao et al., 2012, Lingala and Jacob, 2013]*, [4] *[Gao et al., 2011, Lingala et al., 2011, Otazo et al., 2015, Ravishankar et al., 2017, Babu et al., 2023]*

Prior Works

- **Deep image prior (DIP)-based algorithms[5]**
  - Overfitting
  - May require early stopping or additional regularization

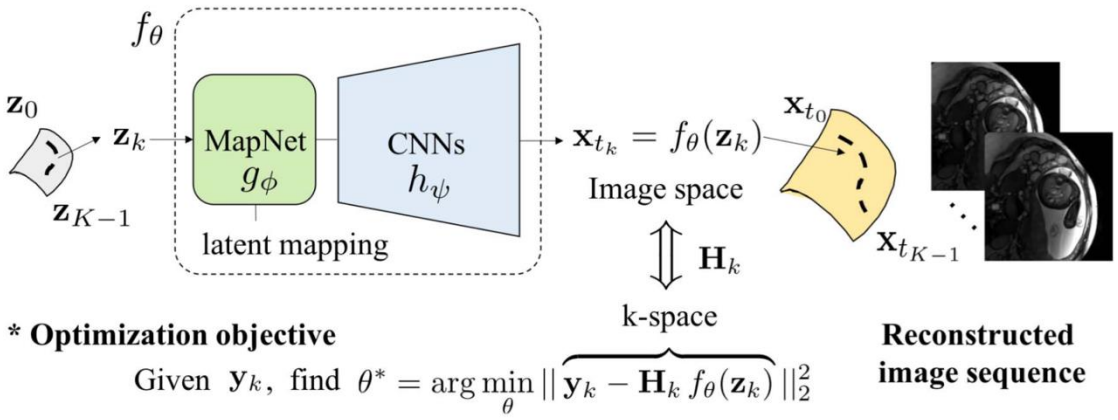

[5] *[Zou et al., 2021, Yoo et al., 2021],* [6] *[Ahmed et al., 2022]*

Prior Works

- **Deep image prior (DIP)-based algorithms[5]**
  - Overfitting
  - May require early stopping or additional regularization

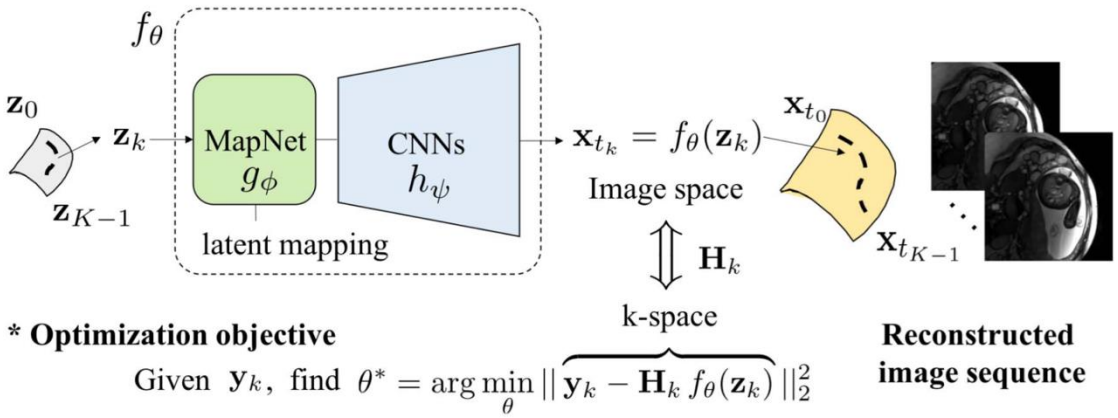

- **Combination of PSM and generative models[6]**
  - May not be easily scalable
  - Overfitting

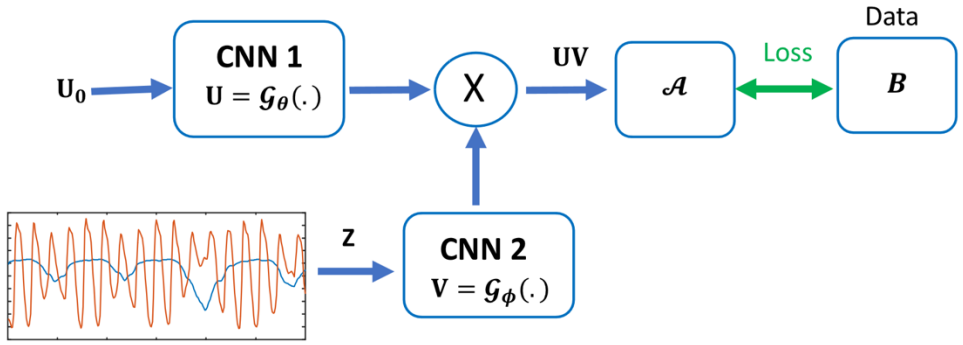

[5] *[Zou et al., 2021, Yoo et al., 2021]*, [6] *[Ahmed et al., 2022]*

Prior Works

- **PSM with pre-learned spatial priors[8]**
  - Improves over previous PSM-based methods and DIP-based generative techniques
  - May not be sufficiently expressive for high-rank objects

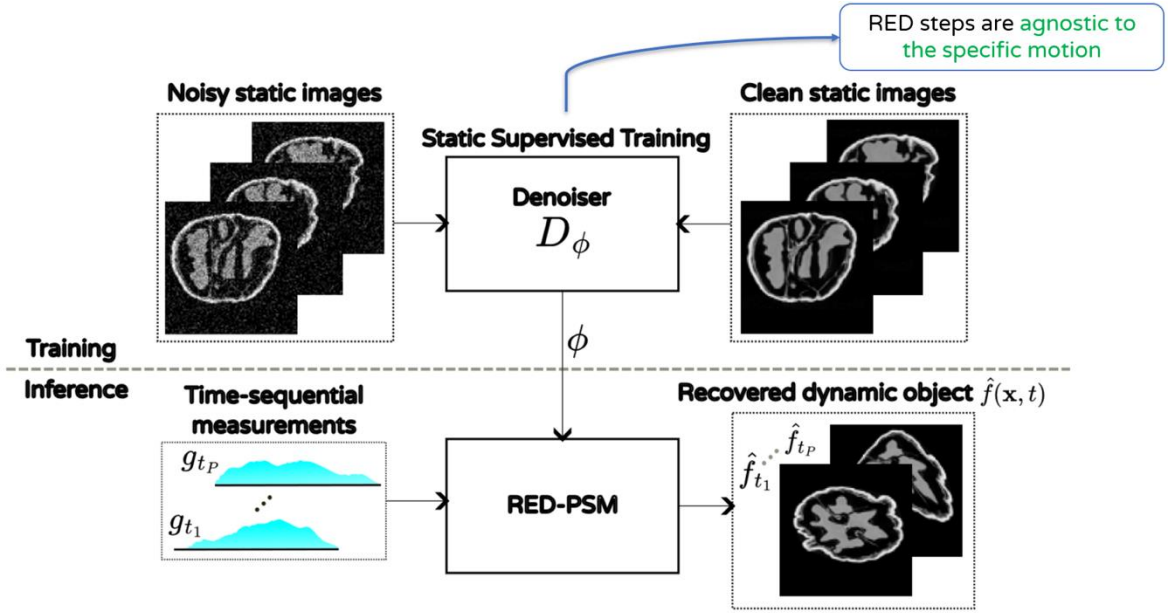

[8] *[Iskender et al., 2024],* [9] *[Reed et al., 2021, Zhang et al., 2023, Shao et al., 2023]*

Prior Works

- **PSM with pre-learned spatial priors[8]**
  - ➢ Improves over previous PSM-based methods and DIP-based generative techniques
  - ➢ May not be sufficiently expressive for high-rank objects

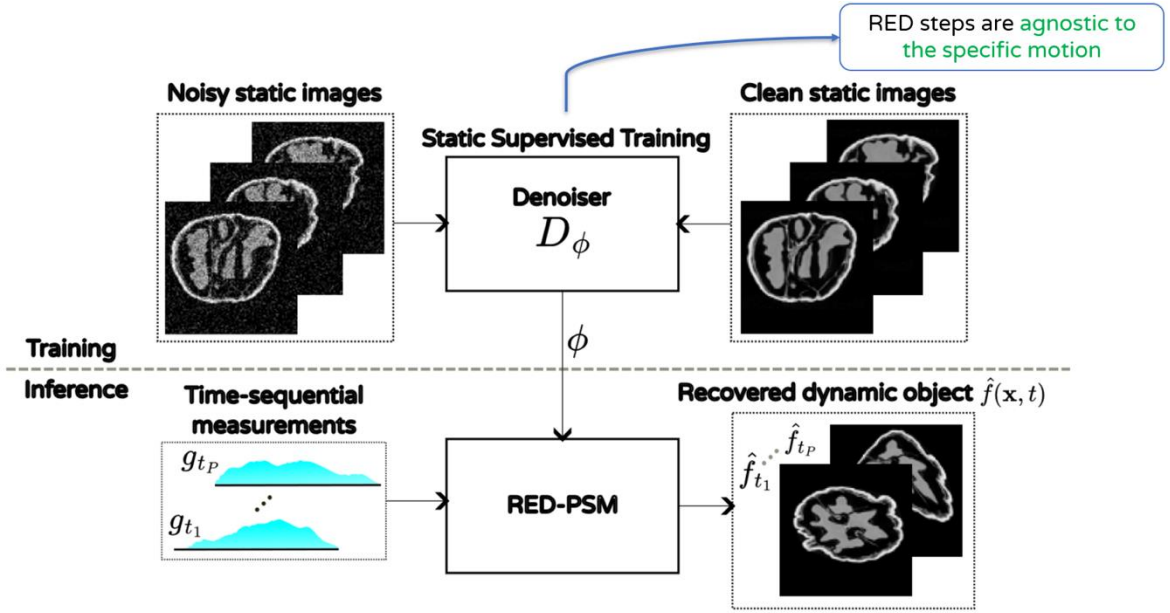

- **Neural field (NF)-based algorithms[9]**
  - ➢ Parsimonious representation
  - ➢ Simple regularization
  - ➢ Static template & motion field decomposition

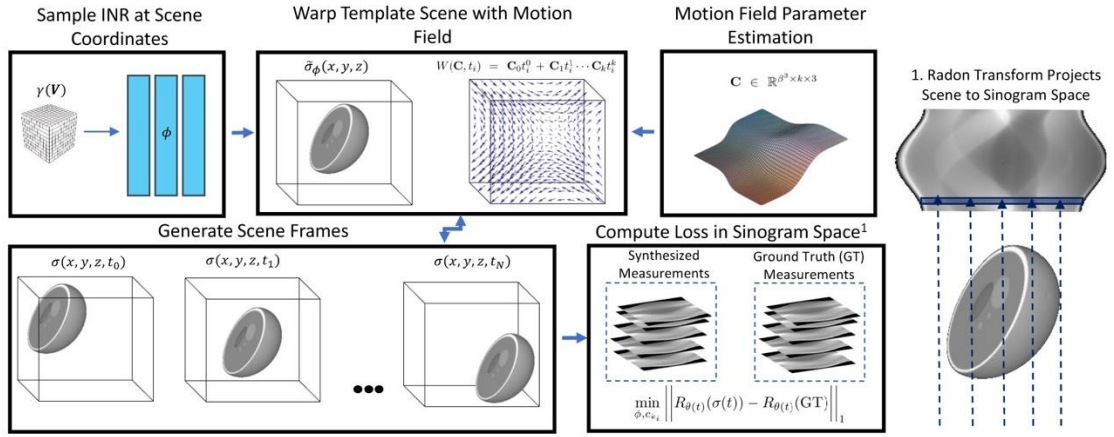

[8] *[Iskender et al., 2024]*, [9] *[Reed et al., 2021, Zhang et al., 2023, Shao et al., 2023]*

RSR-NF: Overview

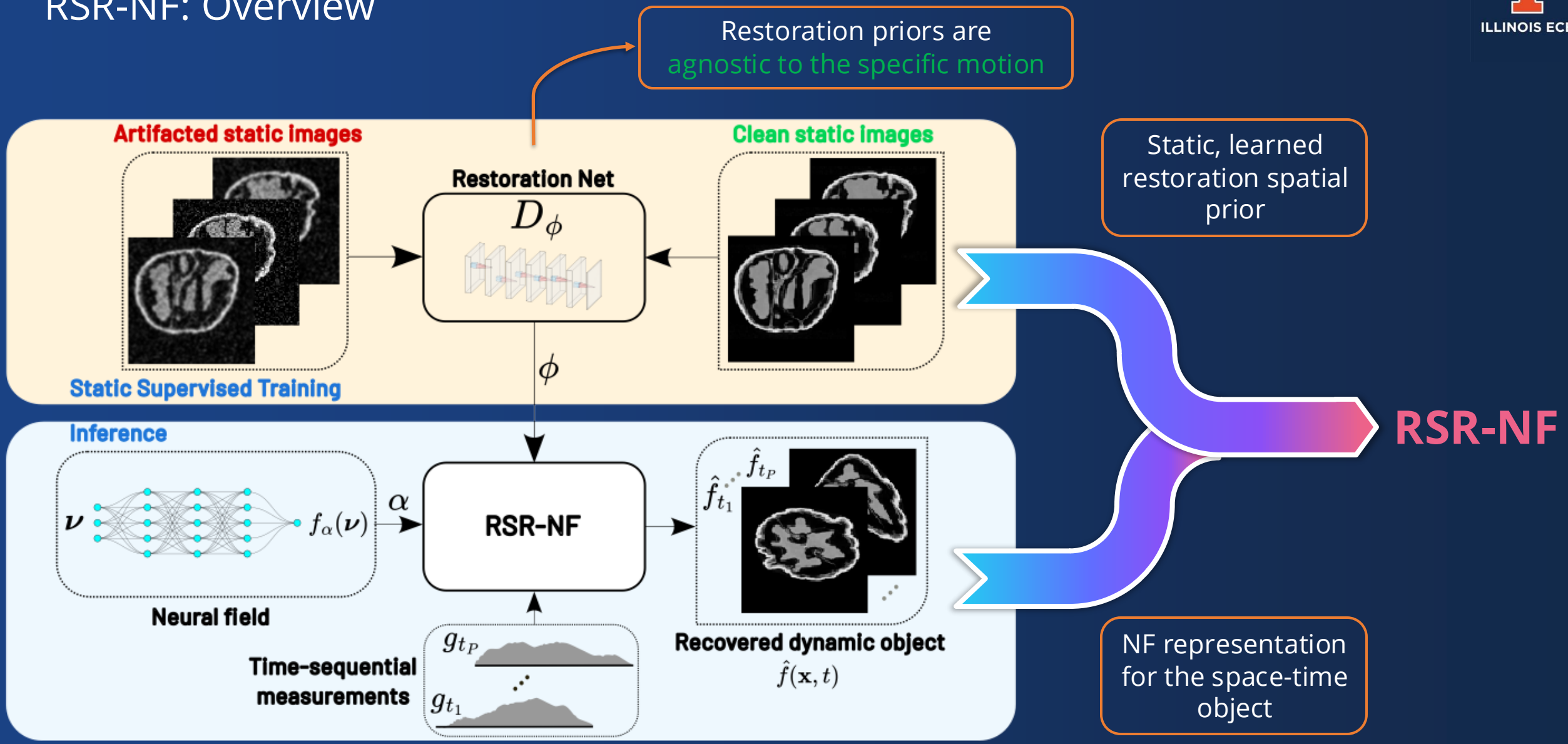

Motivation

- Scarce ground-truth spatio-temporal data ➡ Need for spatial priors

Motivation

ILLINOIS ECE

- Scarce ground-truth spatio-temporal data ➡ Need for spatial priors
- Better spatial priors ➡ improved reconstruction accuracy

Motivation

ILLINOIS ECE

- Scarce ground-truth spatio-temporal data ➡ Need for spatial priors
- Better spatial priors ➡ improved reconstruction accuracy
- Existing object-domain algorithms are not conveniently scalable for high-res 2D/3D + time objects

Motivation

ILLINOIS ECE

- Scarce ground-truth spatio-temporal data ➡ Need for spatial priors
- Better spatial priors ➡ improved reconstruction accuracy
- Existing object-domain algorithms are not conveniently scalable for high-res 2D/3D + time objects
- Hard-constraint low-rank prior not sufficient for highly dynamic objects

Motivation

ILLINOIS ECE

- Scarce ground-truth spatio-temporal data ➡ Need for spatial priors
- Better spatial priors ➡ improved reconstruction accuracy
- Existing object-domain algorithms are not conveniently scalable for high-res 2D/3D + time objects
- Hard-constraint low-rank prior not sufficient for highly dynamic objects
- Existing NF-based methods suffer from limitations related to motion field estimation

Neural Fields (NFs)

- Resolution-free & coordinate-based continuous object representation using DNNs
- Computes output features of an object f at coordinate $\boldsymbol{\nu} \in \mathbb{R}^{d_i}$

$$\underbrace{f^{\alpha}(\boldsymbol{\nu})}_{\text{MLP-based NN } \mathbb{R}^{d_i} \to \mathbb{R}^{d_o} \text{ parameters: } \alpha} = \underbrace{\mu_{\boldsymbol{\nu}}}_{\text{output features, } \in \mathbb{R}^{d_o}}$$

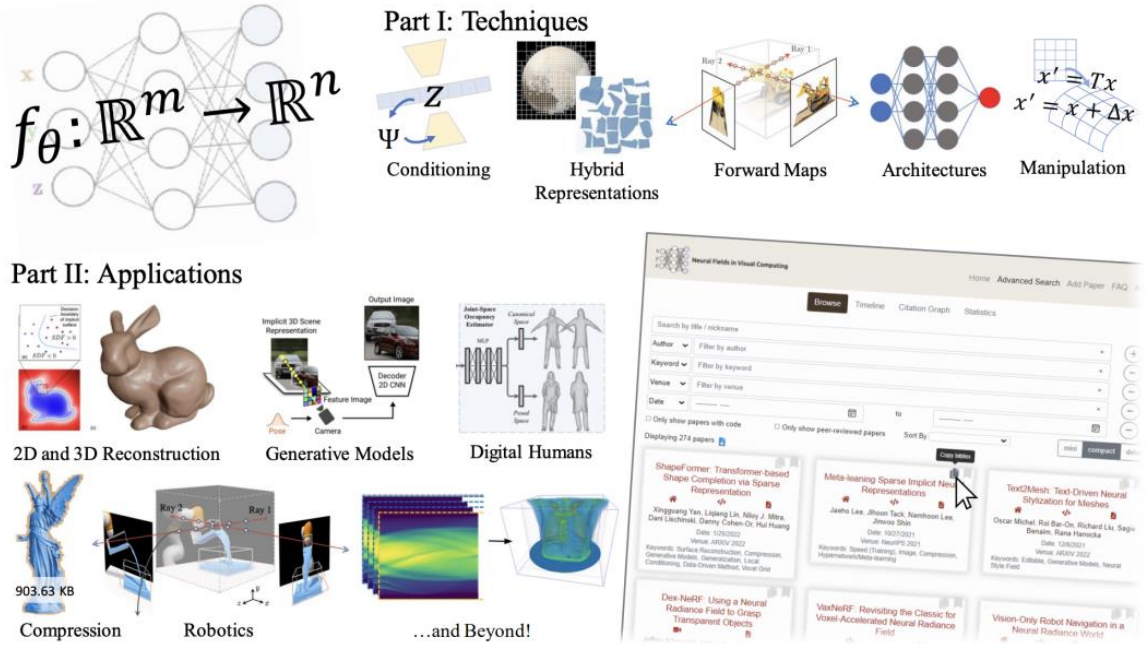

Xie, Yiheng, et al. "Neural fields in visual computing and beyond." Computer graphics forum. Vol. 41. No. 2. 2022.

- Parsimonious: Number of parameters & memory requirements do not directly scale with resolution

RSR-NF: NF Representation for f

Two-stage NF $f^{\alpha}(\boldsymbol{\nu})$ for $\boldsymbol{\nu} \in [0,1]^3$:

RSR-NF: NF Representation for f

ILLINOIS ECE

Two-stage NF $f^{\alpha}(\boldsymbol{\nu})$ for $\boldsymbol{\nu} \in [0,1]^3$:

1. Fourier positional encodings $\gamma(\boldsymbol{\nu}) \in \mathbb{R}^{L\times 6}$ with L linearly increasing frequency components:

$$\gamma(\boldsymbol{\nu})_l = (\sin(\frac{\pi}{2} l\boldsymbol{\nu}), \cos(\frac{\pi}{2} l\boldsymbol{\nu})) \quad \text{where} \quad l \in \{1, \ldots, L\}$$

RSR-NF: NF Representation for f

Two-stage NF $f^{\alpha}(\boldsymbol{\nu})$ for $\boldsymbol{\nu} \in [0,1]^3$:

1. Fourier positional encodings $\gamma(\boldsymbol{\nu}) \in \mathbb{R}^{L\times 6}$ with L linearly increasing frequency components:

$$\gamma(\boldsymbol{\nu})_l = (\sin(\frac{\pi}{2} l\boldsymbol{\nu}), \cos(\frac{\pi}{2} l\boldsymbol{\nu})) \quad \text{where} \quad l \in \{1, \ldots, L\}$$

2. MLP network with ReLU nonlinearity: $M_{\alpha}: \mathbb{R}^{L\times 6} \to \mathbb{R}$

- Overall:

$$f^{\alpha}(\boldsymbol{\nu}) = M_{\alpha}(\gamma(\boldsymbol{\nu})) = \mu_{\boldsymbol{\nu}}$$

Optimized to represent f

Static Restoration Priors

- **Regularization-by-Denoising (RED)[1]:** A recovery method using an image denoiser D_ϕ in the following regularizer:

$$\rho(f_t) = \frac{1}{2} f_t^T (f_t - D_\phi(f_t))$$

$$D_\phi : \mathbb{R}^{J^2} \to \mathbb{R}^{J^2}$$

$$f_t = f(\cdot, \cdot, t)$$

  - Simple gradient rule:* $\nabla \rho(f_t) = f_t - D_\phi(f_t)$
  - **Semi-supervised:** can be trained on relevant ground-truth static data
  - Limited by the denoiser performance

[1] *[Romano et al., 2017], * [Reehorst and Schniter, 2018] provides an alternative score matching-based framework to explain the good performance of RED with denoisers not satisfying original assumptions.*

Static Restoration Priors

- **Restoration priors[3]:** Replaces D_ϕ with a pre-trained deep restoration operator
  - Semi-supervised: can be trained on relevant ground-truth static data
  - Improved static priors: D_ϕ can be trained to mitigate various types and strengths of artifacts in various static restoration scenarios
  - Training objective:

$$\min_{\phi} \sum_{i} \|f_i - D_\phi(\hat{f}_i)\|_F^2 \ s.t. \ \hat{f}_i = H_i f_i + \eta_i, \ \forall i, \qquad \text{where} \qquad H_i = \zeta_i G_i + (1 - \zeta_i) I$$

Degradation operator: Gaussian blur with kernel size $k_i \sim U[0, k_{\max}]$

$\sim U[0, 1]$

[3] *[Hu et al., 2023], [Hu et al., 2024]*

RSR-NF: Variational Formulation

The naïve objective:

$$\min_{\alpha} \sum_{t} \|g_{\theta(t),t} - R_{\theta(t)} f_t^{\alpha}\|_2^2 + \lambda \rho_{D_\phi}(f_t^{\alpha}) + \xi \rho_{\tau}(f^{\alpha})$$

$\lambda \rho_{D_\phi}(f_t^{\alpha})$: Static learned spatial restoration prior, $\lambda > 0$

$\xi \rho_{\tau}(f^{\alpha})$: Temporal smoothness prior

Finite difference approximation to $\|\partial^2 f / \partial t^2\|_F^2$, $\xi > 0$

$$\rho_{\tau}(f^{\alpha}) = \sum_{t=2}^{P-1} \|f_{t-1}^{\alpha} - 2 f_t^{\alpha} + f_{t+1}^{\alpha}\|_2^2$$

RSR-NF: Variational Formulation

ILLINOIS ECE

The naïve objective:

$$\min_{\alpha} \sum_{t} \|g_{\theta(t),t} - R_{\theta(t)} f_t^{\alpha}\|_2^2 + \lambda \rho_{D_\phi}(f_t^{\alpha}) + \xi \rho_{\tau}(f^{\alpha})$$

$\lambda \rho_{D_\phi}(f_t^{\alpha})$: Static learned spatial restoration prior, $\lambda > 0$

$\xi \rho_{\tau}(f^{\alpha})$: Temporal smoothness prior

Finite difference approximation to $\|\partial^2 f / \partial t^2\|_F^2$, $\xi > 0$

$$\rho_{\tau}(f^{\alpha}) = \sum_{t=2}^{P-1} \|f_{t-1}^{\alpha} - 2 f_t^{\alpha} + f_{t+1}^{\alpha}\|_2^2$$

Problem: Costly NF updates through the deep restoration operator D_ϕ in $\rho_{D_\phi}(f_t^{\alpha})$

RSR-NF: Variational Formulation

ILLINOIS ECE

Problem: Costly NF updates through the deep restoration operator D_ϕ in $\rho_\phi(f_t^\alpha)$

Solution: Variable split $f^\alpha = \bar{f}$

RSR-NF: Variational Formulation

ILLINOIS ECE

Problem: Costly NF updates through the deep restoration operator D_ϕ in $\rho_\phi(f_t^\alpha)$

Solution: Variable split $f^\alpha = \bar{f}$

The final objective:

$$\min_{\alpha, \bar{f}} \sum_t \|g_{\theta(t),t} - R_{\theta(t)} f_t^\alpha\|_2^2 + \lambda \rho_{D_\phi}(\bar{f}_t) + \xi \rho_\tau(f^\alpha)$$

$$\text{s.t. } f^\alpha = \bar{f}$$

- Estimated reconstruction → f^α

RSR-NF: ADMM Optimization Algorithm

input: $\alpha^{(0)},\ \bar{f}^{(0)} = f_{\alpha}^{(0)},\ \gamma^{(0)},\ \beta > 0,\ \lambda > 0,\ \xi > 0$

for $i \in \{1, \ldots, I\}$ **do**

$$\alpha^{(i)} = \arg\min_{\alpha} \{ \textstyle\sum_t \| g(\cdot, \theta(t), t) - R_{\theta(t)} f_t^{\alpha} \|_2^2 + \frac{\beta}{2} \| f_t^{\alpha} + \gamma_t^{(i-1)} - \bar{f}_t^{(i-1)} \|_F^2 + \xi \rho_{\tau}(f^{\alpha}) \}$$

$$\forall t: \ \bar{f}_t^{(i)} = \tfrac{\lambda}{\lambda+\beta} D_{\phi}(\bar{f}_t^{(i-1)}) + \tfrac{\beta}{\lambda+\beta} \left(f_t^{\alpha(i)} + \gamma_t^{(i-1)} \right)$$

$$\gamma^{(i)} = \gamma^{(i-1)} + f^{\alpha(i)} - \bar{f}^{(i)}$$

end for

Single fixed-point iteration to optimize w.r.t $\bar{f}_t^{(i)}$

RSR-NF: Overview

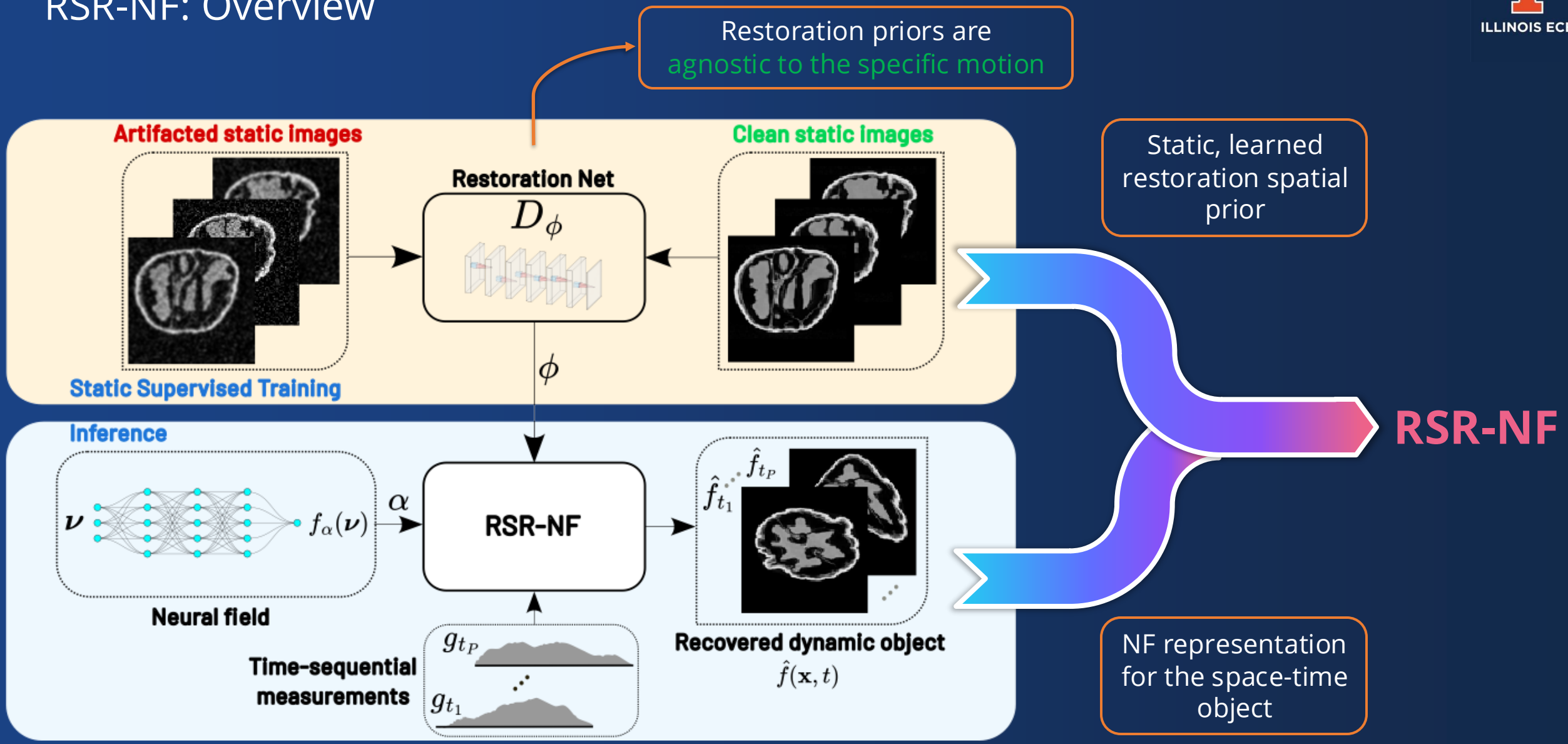

Experiments: Test Data & Acquisition Scheme

- **Accuracy Benchmark**: Ground-truth object at each frame

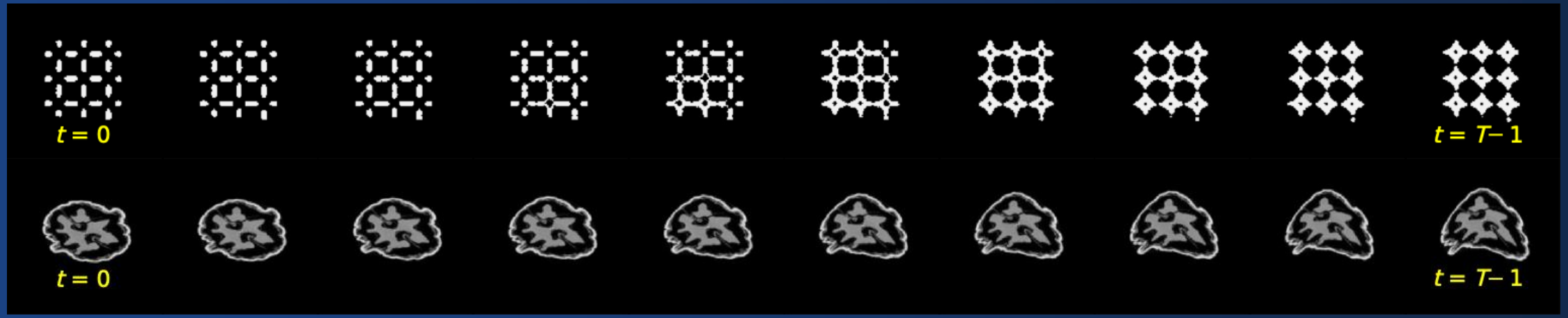

- **Comparison Benchmarks:**

1. Temp-NF: RSR-NF without spatial regularization ($\lambda = 0$)
2. RED-PSM [7]: PSM objective with pre-learned denoiser-based prior
3. TD-DIP [8]: a recent deep image prior (DIP)-based method for MRI recon

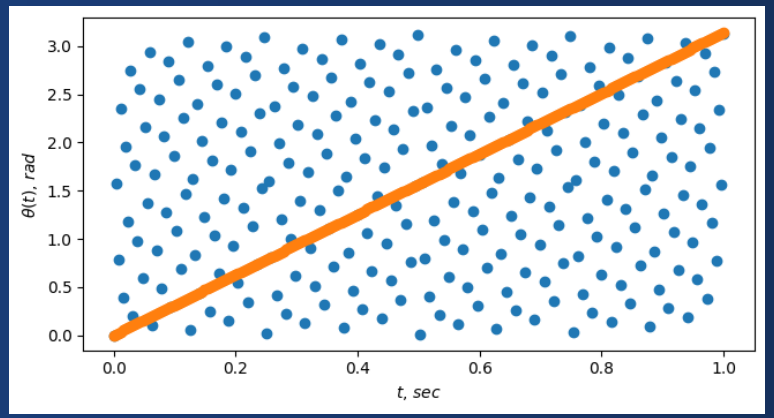

Acquisition: Bit-reversed angular sampling over $[0, \pi]$

Reconstructions from time-sequential projections: Accuracies

ILLINOIS ECE

- Reconstruction accuracies vs. total number of projections P:

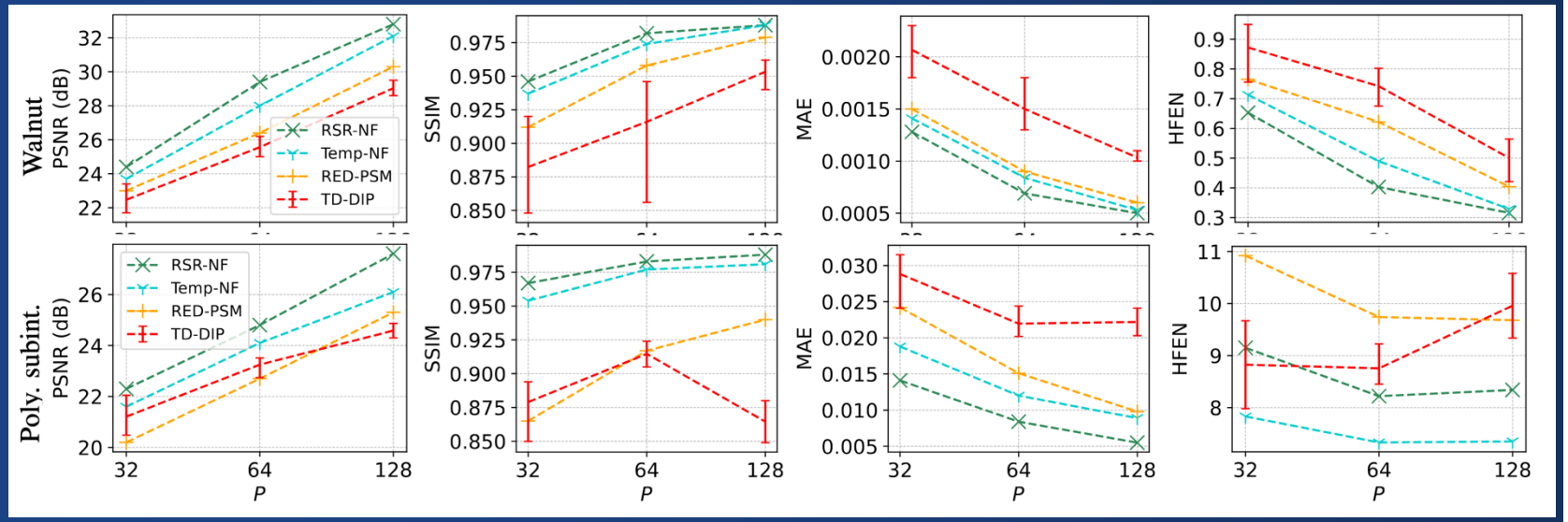

- Reconstruction PSNR vs. t:

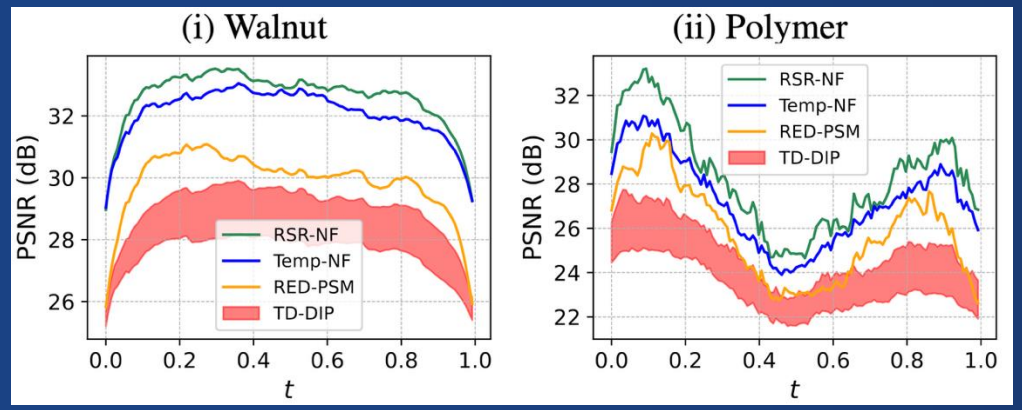

Consistent improvements over comparison benchmarks

	P	Method	PSNR (dB)	SSIM	MAE (1e-3)	HFEN
Walnut	32	FBP	15.1	0.300	8.4	2.13
		TD-DIP (L)	22.5	0.882	2.1	0.87
		RED-PSM	22.8	0.911	1.5	0.78
		Temp-NF	23.7	0.937	1.4	0.71
		RSR-NF	**24.4**	**0.946**	**1.3**	**0.65**
	64	FBP	18.3	0.387	5.4	2.04
		TD-DIP (L)	25.6	0.916	1.5	0.74
		RED-PSM	26.4	0.958	0.9	0.57
		Temp-NF	28.0	0.974	0.8	0.49
		RSR-NF	**29.4**	**0.982**	**0.7**	**0.40**
	128	FBP	20.3	0.503	3.8	2.22
		TD-DIP (L)	29.0	0.953	1.0	0.50
		RED-PSM	30.3	0.979	0.6	0.40
		Temp-NF	32.1	0.988	0.5	0.33
		RSR-NF	**32.8**	**0.988**	**0.5**	**0.32**
Polymer	32	FBP	9.6	0.292	22.69	50.1
		TD-DIP (L)	21.1	0.850	3.09	9.67
		RED-PSM	20.2	0.865	2.42	10.92
		Temp-NF	21.6	0.954	1.88	9.15
		RSR-NF	**22.3**	**0.967**	**1.41**	**7.83**
	64	FBP	14.4	0.352	12.30	35.6
		TD-DIP (L)	23.5	0.915	2.13	8.59
		RED-PSM	22.7	0.917	1.51	9.74
		Temp-NF	24.1	0.977	1.20	8.22
		RSR-NF	**24.8**	**0.983**	**0.84**	**7.33**
	128	FBP	17.1	0.466	7.64	31.49
		TD-DIP (L)	24.3	0.849	2.41	10.58
		RED-PSM	25.3	0.940	0.98	9.68
		Temp-NF	26.8	0.986	0.74	8.31
		RSR-NF	**27.6**	**0.988**	**0.55**	**7.35**

$$\mathrm{HFEN}(f, f_r) = \|\mathrm{LoG}(f) - \mathrm{LoG}(f_r)\|_2$$

Reconstructions from time-sequential projections: Walnut

ILLINOIS ECE

- $x - y$ slices:

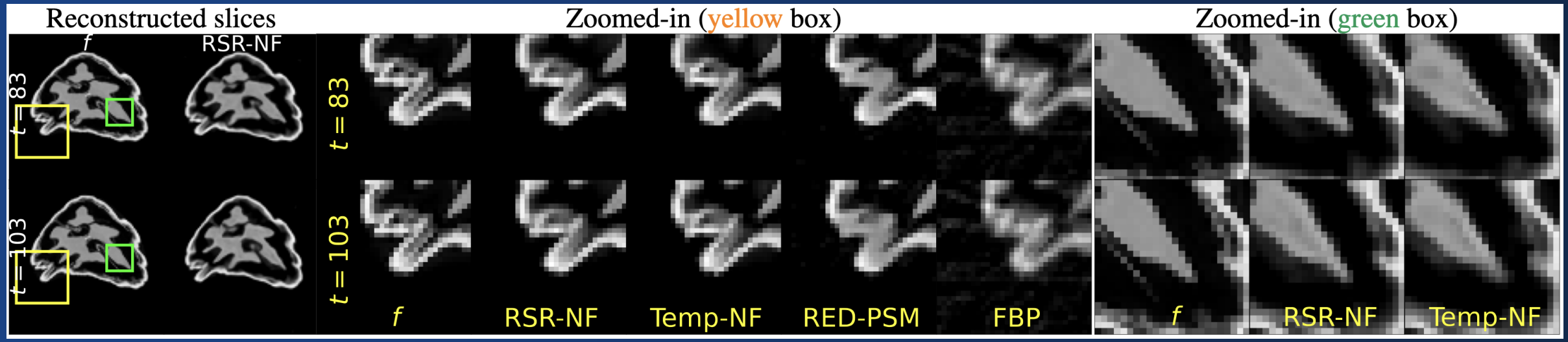

Improved recovery of high-frequency features and uniform density regions

- $x - t$ slices:

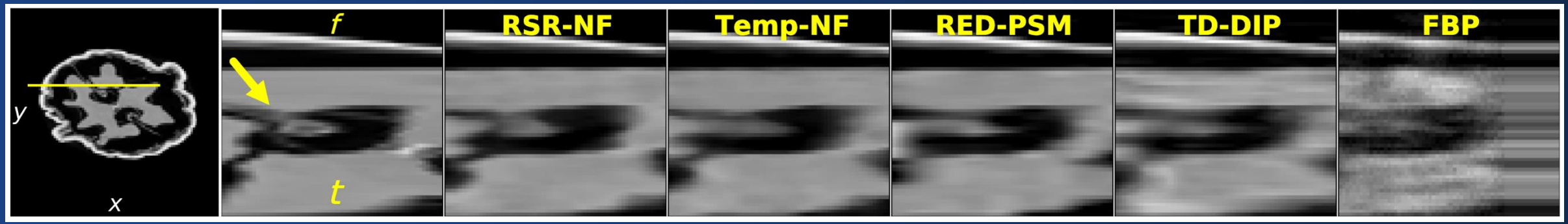

Higher temporal resolution

Reconstructions from time-sequential projections: Compressed Polymer

ILLINOIS ECE

- $x - y$ slices:

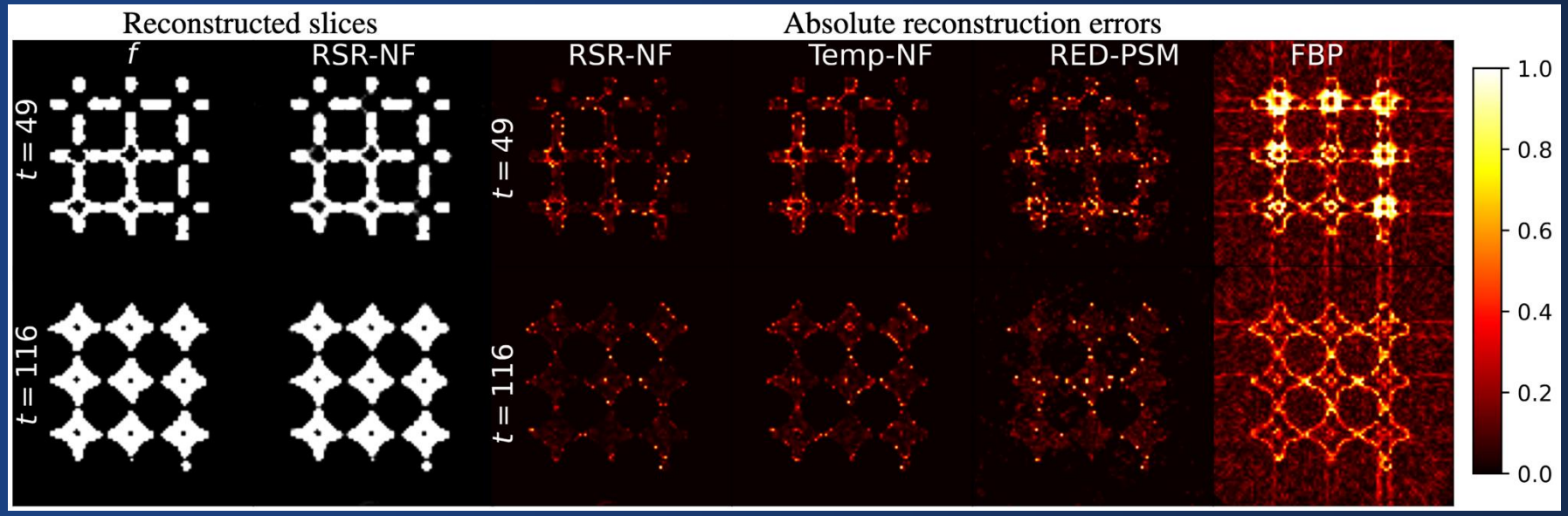

Improved reconstruction accuracies

- $x - t$ slices:

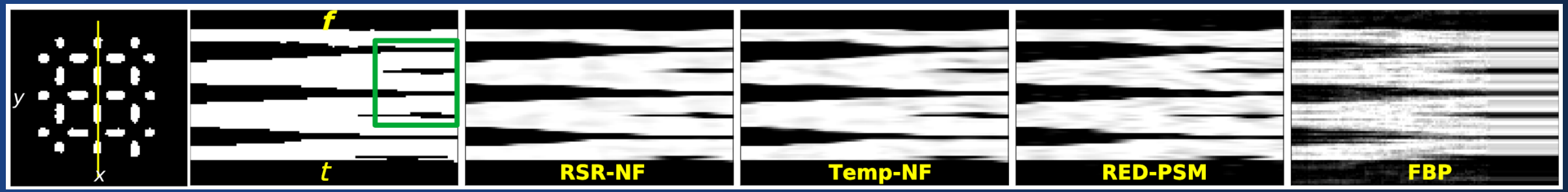

Higher temporal resolution

Conclusions

1. The first NF-based dynamic imaging method with pre-learned spatial priors

Conclusions

ILLINOIS ECE

1. The first NF-based dynamic imaging method with pre-learned spatial priors
2. A computationally efficient ADMM algorithm avoiding costly backpropagation through the deep regularizer NN for NF updates

Conclusions

ILLINOIS ECE

1. The first NF-based dynamic imaging method with pre-learned spatial priors
2. A computationally efficient ADMM algorithm avoiding costly backpropagation through the deep regularizer NN for NF updates
3. Improved reconstruction accuracies compared to (i) a recent PSM-based alternative, (ii) a DIP-based method, (iii) a NF-based method with only temporal regularization

Conclusions

ILLINOIS ECE

1. The first NF-based dynamic imaging method with pre-learned spatial priors
2. A computationally efficient ADMM algorithm avoiding costly backpropagation through the deep regularizer NN for NF updates
3. Improved reconstruction accuracies compared to (i) a recent PSM-based alternative, (ii) a DIP-based method, (iii) a NF-based method with only temporal regularization
4. Applicable to other dynamic imaging scenarios with scarce ground-truth spatio-temporal data

References

1. Danad, I., Szymonifka et al.,(2016). Static and dynamic assessment of myocardial perfusion by computed tomography. European Heart Journal-Cardiovascular Imaging, 17(8), 836-844.
2. Scanziani, A., Singh, et al. In situ characterization of immiscible three-phase flow at the pore scale for a water-wet carbonate rock. Advances in Water Resources, 121, 446-455, 2018.
3. O'connor, J. P. B., Tofts, P. S., Miles, K. A., Parkes, L. M., Thompson, G., & Jackson, A. (2011). Dynamic contrast-enhanced imaging techniques: CT and MRI. The British journal of radiology, 84, S112-S120.
4. Maire, E., Le Bourlot, C., Adrien, J., Mortensen, A., & Mokso, R. (2016). 20 Hz X-ray tomography during an in situ tensile test. International Journal of Fracture, 200, 3-12.
5. Patterson, Brian M., et al. "In situ X-ray synchrotron tomographic imaging during the compression of hyper-elastic polymeric materials." Journal of materials science 51 (2016): 171-187.
6. Iskender, Berk, Marc L. Klasky, and Yoram Bresler. "RED-PSM: Regularization by denoising of factorized low rank models for dynamic imaging." IEEE Transactions on Computational Imaging, 2024.
7. C. Jailin and S. Roux, “Dynamic tomographic reconstruction of deforming volumes,” Materials, vol. 11, no. 8, 2018, issn: 1996-1944. doi: 10.3390/ma11081395.
8. C. Jailin et al., “Projection-based dynamic tomography,” Phys. Med. Biol., vol. 66, no. 21, p. 215 018, 2021.
9. G. Zang et al., “Space-time tomography for continuously deforming objects,” ACM Transactions on Graphics, 2018.
10. S. Capostagno et al., “Deformable motion compensation for interventional cone-beam CT,” Phys. Med. Biol., vol. 66, no. 5, p. 055 010, Feb. 2021.
11. M. Burger et al., “A variational reconstruction method for undersampled dynamic x-ray tomography based on physical motion models,” Inverse Problems, 2017.
12. B. N. Hahn et al., “Using the Navier-Cauchy equation for motion estimation in dynamic imaging,” Inverse Problems and Imaging, vol. 16, no. 5, p. 1179, 2022. doi:10.3934/ipi.2022018.
13. Z.-P. Liang, “Spatiotemporal imaging with partially separable functions,” in 2007 4th IEEE international symposium on biomedical imaging: from nano to macro, IEEE, 2007, pp. 988–991.
14. J. P. Haldar and Z.-P. Liang, “Low-rank approximations for dynamic imaging,” in 2011 IEEE International Symposium on Biomedical Imaging: From Nano to Macro, IEEE, 2011, pp. 1052–1055.
15. B. Zhao et al., “Further development of image reconstruction from highly undersampled (k, t)-space data with joint partial separability and sparsity constraints,” IEEE ISBI, 2011.
16. S. G. Lingala and M. Jacob, “Blind compressive sensing dynamic MRI,” IEEE transactions on medical imaging, vol. 32, no. 6, pp. 1132–1145, 2013.
17. H. Gao, J.-F. Cai, Z. Shen, and H. Zhao, “Robust principal component analysis-based four-dimensional computed tomography,” Physics in Medicine & Biology, vol. 56, no. 11, p. 3181, 2011.
18. S. G. Lingala et al., “Accelerated dynamic MRI exploiting sparsity and low-rank structure: Kt SLR,” IEEE transactions on medical imaging, vol. 30, no. 5, pp. 1042–1054, 2011.
19. R. Otazo, E. Candes, and D. K. Sodickson, “Low-rank plus sparse matrix decomposition for accelerated dynamic MRI with separation of background and dynamic components,” Mag. Res. in Med., 2015.
20. S. Ravishankar et al., “Low-rank and adaptive sparse signal (LASSI) models for highly accelerated dynamic imaging,” IEEE transactions on medical imaging, vol. 36, no. 5, pp. 1116–1128, 2017.
21. S. Babu, S. G. Lingala, and N. Vaswani, “Fast low rank column-wise compressive sensing for accelerated dynamic MRI,” IEEE Transactions on Computational Imaging, 2023.
22. Q. Zou, A. H. Ahmed, P. Nagpal, S. Kruger, and M. Jacob, “Dynamic imaging using a deep generative storm (gen-storm) model,” IEEE transactions on medical imaging, vol. 40, no. 11, pp. 3102–3112, 2021.
24. J. Yoo, K. H. Jin, H. Gupta, J. Yerly, M. Stuber, and M. Unser, “Time-dependent deep image prior for dynamic mri,” IEEE Transactions on Medical Imaging, vol. 40, no. 12, pp. 3337–3348, 2021.
25. A. H. Ahmed, Q. Zou, P. Nagpal, and M. Jacob, “Dynamic imaging using deep bi-linear unsupervised representation (deblur),” IEEE Transactions on Medical Imaging, vol. 41, no. 10, pp. 2693–2703, 2022.

References

26. A. W. Reed, et al., “Dynamic CT reconstruction from limited views with implicit neural representations and parametric motion fields,” IEEE/CVF ICCV, 2021.
27. Y. Zhang et al., “Dynamic cone-beam CT reconstruction using spatial and temporal implicit neural representation learning (STINR),” Physics in Medicine & Biology, vol. 68, no. 4, p. 045 005, 2023.
28. H.-C. Shao, T. Mengke, T. Pan, and Y. Zhang, “Dynamic CBCT imaging using prior model-free spatiotemporal implicit neural representation (pmf-stinr),” ArXiv, 2023.
29. E. D. Zhong, T. Bepler, J. H. Davis, and B. Berger, “Reconstructing continuous distributions of 3d protein structure from cryo-em images,” arXiv preprint arXiv:1909.05215, 2019.
30. Y. Romano, M. Elad, and P. Milanfar, “The little engine that could: Regularization by denoising (red),” SIAM Journal on Imaging Sciences, vol. 10, no. 4, pp. 1804–1844, 2017.
31. E. T. Reehorst and P. Schniter, “Regularization by denoising: Clarifications and new interpretations,” IEEE transactions on computational imaging, vol. 5, no. 1, pp. 52–67, 2018.
32. Y. Hu et al., “A restoration network as an implicit prior,” arXiv preprint arXiv:2310.01391, 2023.
33. Y. Hu et al., “Stochastic deep restoration priors for imaging inverse problems,” arXiv preprint arXiv:2410.02057, 2024.

Thank you!

Limited number of distinct views

ILLINOIS ECE

Physical challenge: Accessing a complete set of distinct view angles in bit-reversed order

Easier to implement: Smaller number of distinct view angles $\hat{P}$, repeated periodically s.t. $\mathrm{P} = 128$

Acquisition: Bit-reversed angular sampling over $[0, \pi]$

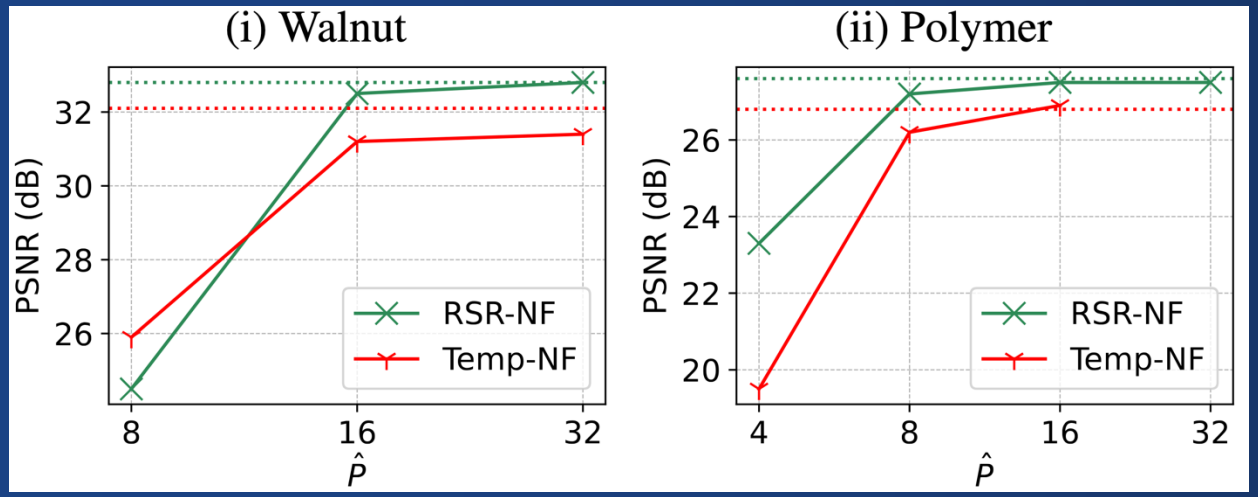

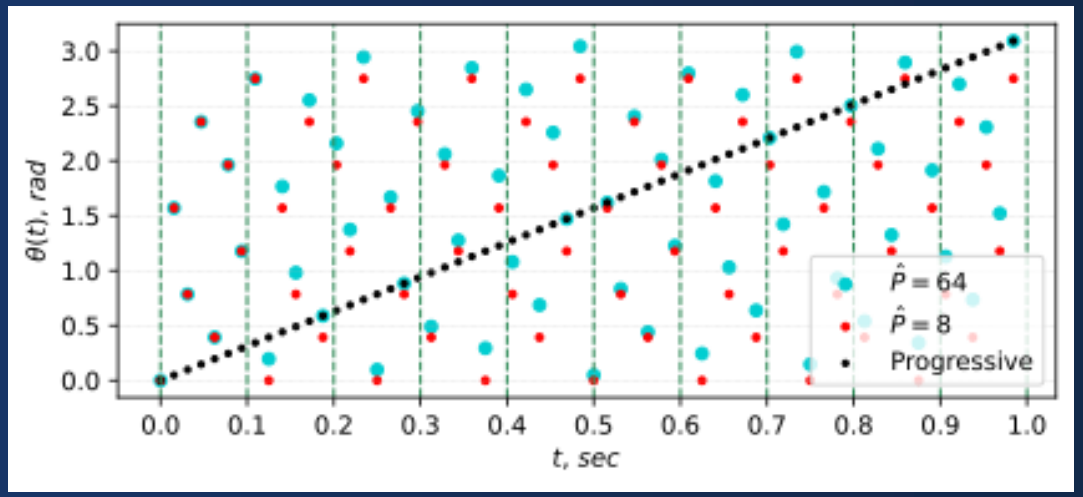

RSR-NF is increasingly robust to decrease in # of distinct view angles for $\hat{P} > 8$

Both methods robust to decrease for $\hat{P} > 8$

Temp-NF with sharper decline for $\hat{P} = 4$

Testing the accuracy of the representation: Embedding Experiments

ILLINOIS ECE

Comparison on polymer subinterval:

1. The proposed NF
2. Low-rank PSM

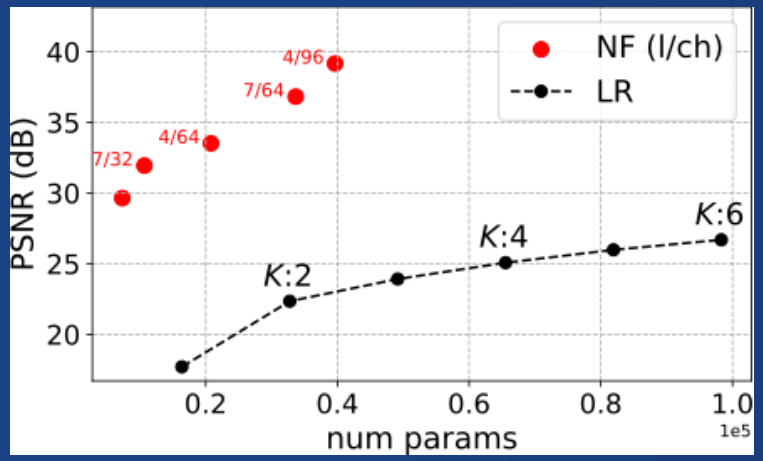

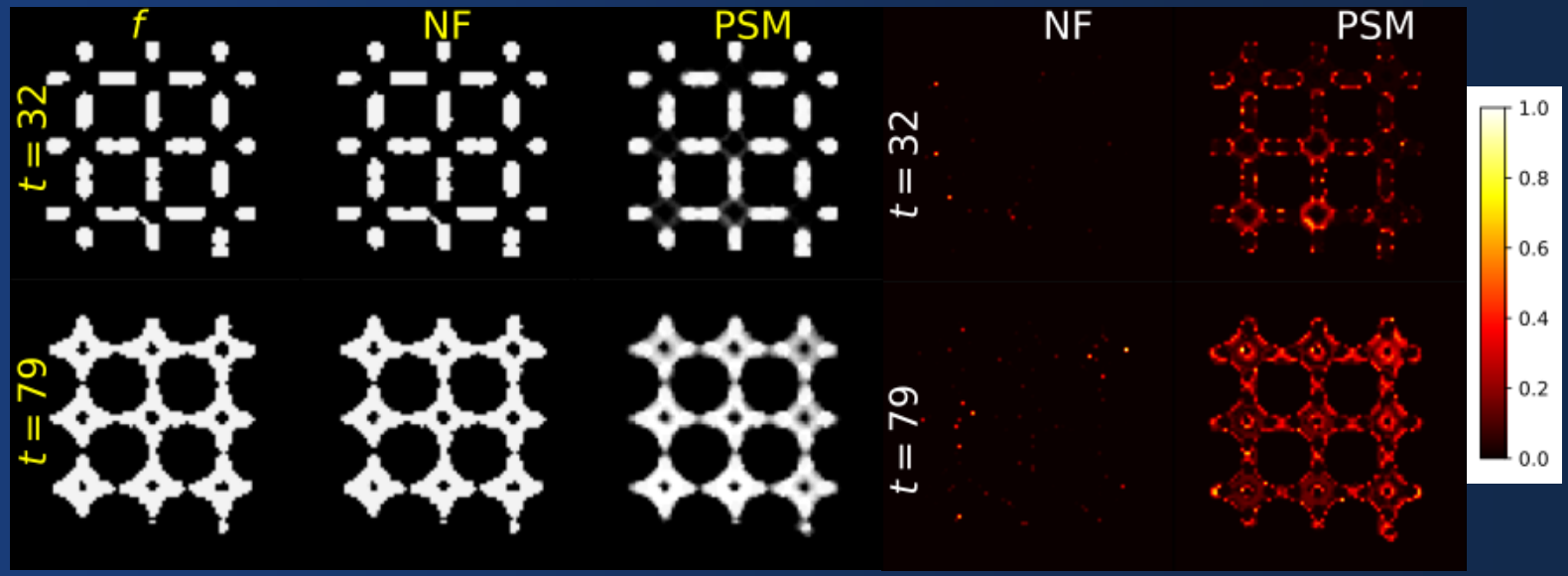

Representation PSNRs: NF ≫ PSM

Slices represented with similar number of free parameters:

- NF: 7 layers & 64 channels per layer
- rank(PSM) = 3

PSM leads to over-smoothed representations compared to NF

Prior Works

- **Deep image prior (DIP)-based algorithms[5]**
  - Overfitting
  - May require early stopping or additional regularization

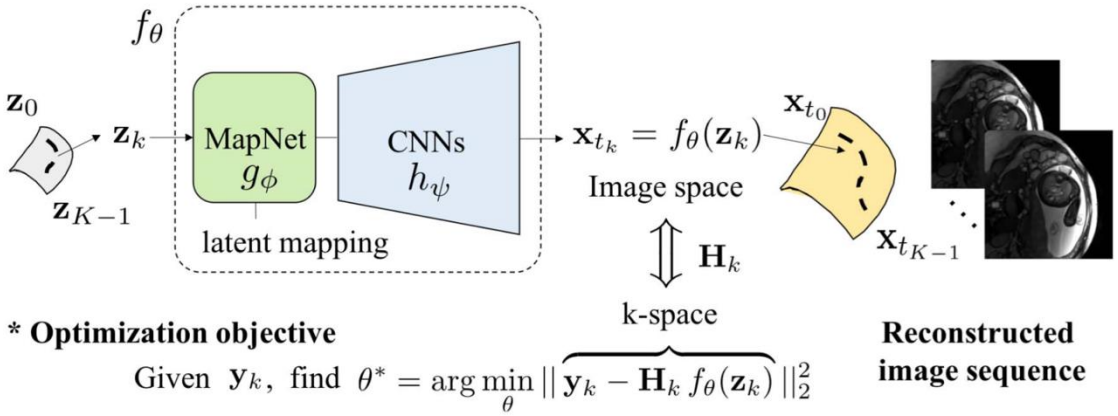

- **Combination of PSM and generative models[7]**
  - May not be easily scalable
  - Overfitting

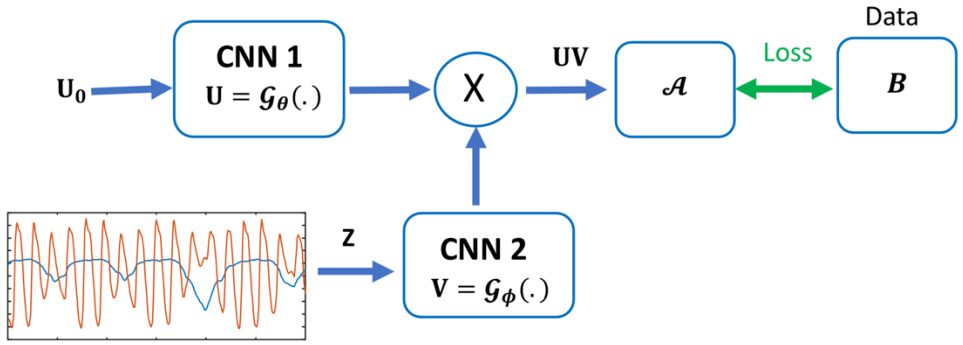

- **Manifold models[6]**
  - Require spatio-temporal training data for reconstruction

[5] *[Zou et al., 2021, Yoo et al., 2021]*, [6] *[Djebra et al., 2022]*, [7] *[Ahmed et al., 2022]*

RSR-NF: Algorithm

input: $\alpha^{(0)}$, $\bar{f}^{(0)} = \tilde{f}_{\alpha}^{(0)}$, $\gamma^{(0)}$, $\beta > 0$, $\lambda > 0$, $\xi > 0$

for $i \in \{1, \ldots, I\}$ **do**

$$\alpha^{(i)} = \arg\min_{\alpha} \{ \sum_t \| g(\cdot, \theta(t), t) - R_{\theta(t)} \tilde{f}_t^{\alpha} \|_2^2 + \frac{\beta}{2} \| \tilde{f}_t^{\alpha} + \gamma_t^{(i-1)} - \bar{f}_t^{(i-1)} \|_F^2 + \xi \rho_{\tau}(\tilde{f}^{\alpha}) \}$$

$$\forall t: \quad \bar{f}_t^{(i)} = \arg\min_{\bar{f}_t} \{ \lambda \rho(\bar{f}_t) + \frac{\beta}{2} \| (\tilde{f}^{\alpha(i)} + \gamma^{(i-1)}) e_t - \bar{f}_t \|_2^2 \}$$

$$\gamma^{(i)} = \gamma^{(i-1)} + \tilde{f}^{\alpha(i)} - \bar{f}^{(i)}$$

end for

Iterative solution → many forward passes over deep D_{ϕ}

Experiments: Test Data & Acquisition Scheme

ILLINOIS ECE

- **Accuracy Benchmark**: Ground-truth object at each frame

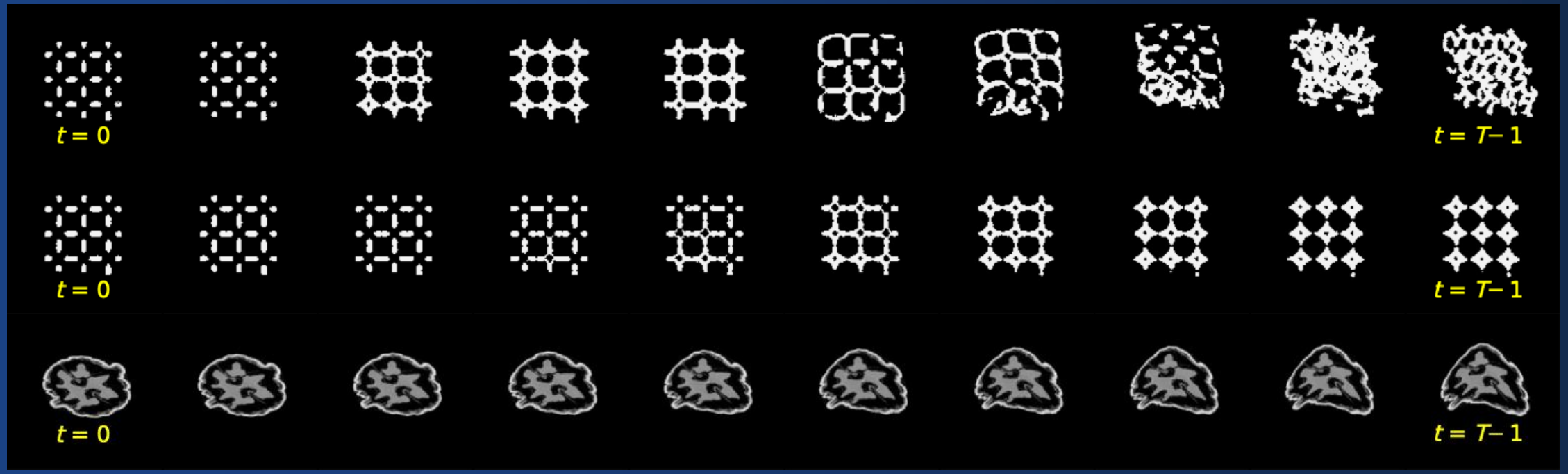

- **Comparison Benchmarks:**

1. Temp-NF: RSR-NF without spatial regularization ($\lambda = 0$)
2. RED-PSM [7]: PSM objective with pre-learned denoiser-based prior
3. TD-DIP [8]: a recent deep image prior (DIP)-based method for MRI recon

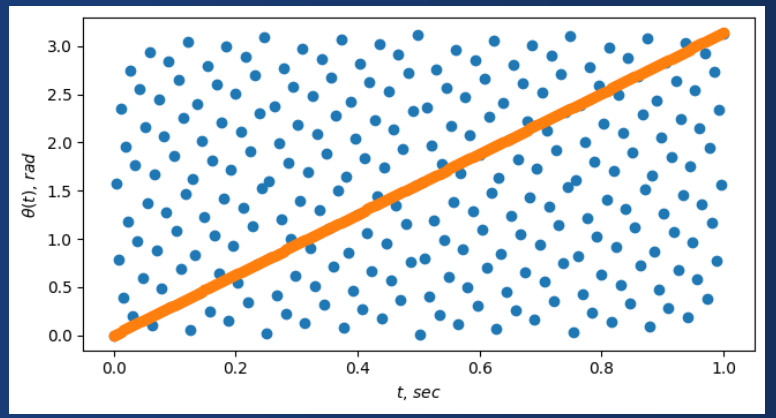

Acquisition: Bit-reversed angular sampling over $[0, \pi]$